Low Temperature Growth of Carbon Nanotube Forests Consisting of Tubes with Narrow Inner Spacing Using Co/Al/Mo Catalyst on Conductive Supports

Hisashi Sugime*,[1], Santiago Esconjauregui,[1] Lorenzo D'Arsié,[1] Junwei Yang,[1] Alex W. Robertson,[2] Rachel A. Oliver,[3] Sunil Bhardwaj,[4,5] Cinzia Cepek,[4] John Robertson[1]

[1]Department of Engineering, University of Cambridge, Cambridge CB3 0FA, United Kingdom
[2]Department of Materials, University of Oxford, Parks Road, OX1 3PH, UK
[3]Department of Materials Science and Metallurgy, University of Cambridge, Cambridge CB2 3QZ, United Kingdom
[4]Istituto Officina dei Materiali-CNR, Laboratorio TASC, Trieste I-34149, Italy
[5]Sincrotrone Trieste S.C.p.A., Strada Statale 14, Km 163.5, Trieste I-34149, Italy

ABSTRACT

We grow carbon nanotube forests at 450 °C on conductive Cu support with tubes exhibiting extremely narrow inner spacing using Co/Al/Mo multilayer catalyst system. The forests average ~300 nm in height and a mass density of 1.2 g cm^{-3}. As a barrier layer for the diffusion of Co, the thin Al layer with the thickness of 0.5 nm plays an important role in the growth of dense CNT forests, partially preventing the Co-Mo interaction. Ohmic conduction is confirmed between the forest and Cu support with the resistance of 35 ± 26 kΩ (mean ± standard deviation). The forest shows a high thermal effusivity of 1840 J m^{-2} $s^{-0.5}$ K^{-1}, and a thermal conductivity of 4.0 J s^{-1} m^{-1} K^{-1}, suggesting that these forests are potentially useful for heat dissipation devices.

1. Introduction

Carbon nanotubes (CNTs) are envisaged as the building block in wide range of industries due to their outstanding mechanical, electrical, and thermal properties.[1-4] For these applications to materialise, however, it is necessary to control the synthesis, to tailor the structure and properties, and do it in an inexpensive way. From the various morphologies obtained in the synthesis, vertically-aligned CNT forests are the form that hold most high-tech industrial potential applications, such as interconnects in next generation electronics and

heat dissipation devices.[5-7] Forests are typically synthesized by chemical vapor deposition (CVD) as it is the only method that can be scaled up in industries, among other reasons because of the relatively low process temperature. Especially for the CMOS compatible processes, the process temperature needs to be lower than 450 °C, while it is typically 700 - 800 °C. In order to realize such low temperature growth of the CNT forests, many groups have reported the optimization of both CVD and catalyst conditions.[8-12]

On the other hand, integrating as many carbon walls as possible in a limited space of CNT forests is another important issue. A larger number of carbon walls is preferred for applications, since each wall behaves as electrical or thermal channel when they are properly contacted.[13] In order to realize this, there are two possible ways. One is reducing the outer spacing (spacing between tubes), and the other one is reducing inner spacing (spacing within each tube). When the outer diameter of the tubes is fixed, the outer spacing can be reduced by increasing area density, while the inner spacing can be reduced by increasing wall number per tube.

In this work, to realize the latter way, we design and engineer the catalyst/supports systems. To date, multi-layer or binary catalysts, which drastically enhance the height or the density of the forest, are widely studied. Aluminium oxide layer, typically with the thickness of 10 - 20 nm, is often used to get high CNT forest up to millimetre scale combining with Fe or Co.[14-19] As for area density, an ultra-high area density single-wall CNT (SWCNT) forest is realized at 750 °C with Al_2O_3/Fe/Al_2O_3 system.[20] On the other hand, Mo is also used to grow CNT forests combining with Fe or Co.[21-24] Especially, Co-Mo binary catalyst is known as the first combination to grow SWCNT forests.[21] Co and Mo form a complex carbide or oxide which keeps Co catalyst particles small.[25-26]

Recently, using Co-Mo catalyst, we have achieved the growth of CNT forests on conductive Ti-coated Cu supports at 450 °C with a record high mass density of 1.6 g cm^{-3}.[27-28] X-ray photoelectron spectroscopy (XPS) shows that Co-Mo-Ti interaction prevents Co nanoparticles from sintering, and plays an important role for the root growth mechanism. In this paper, by extending the concept of multilayer catalyst systems, we demonstrate the growth of a CNT forests consisting of tubes with extremely narrow inner spacing. We use a thin Al barrier layer between Co and Mo layer which enhances the forest growth. The forest grown at 450 °C shows thermal effusivity of 1840 J m^{-2} $s^{-0.5}$ K^{-1}, and thermal conductivity of 4.0 J s^{-1} m^{-1} K^{-1}, suggesting that the forest is potentially useful for the heat dissipation devices. We also confirm an ohmic behavior between the forest and Cu support with the resistance of 35 ± 26 kΩ (mean ± standard deviation), showing that the forest and the conductive support

have a good electrical contact. This new concept of multilayer catalyst system with barrier layer will widen the possibility of designing the catalyst/underlayer systems for the growth of CNT forests.

2. Experimental

2.1 *Catalyst preparation and CNT forest growth*

We first deposit 40 nm Cu as a conductive support followed by 5.0 nm Mo on a SiO_2(200nm)/Si(100) substrate. Then, we deposit 0.25, 0.50, or 1.0 nm Al followed by 2.5 nm Co. As reference, we also prepare samples without Al and/or Mo. All metal depositions are carried out by DC magnetron sputtering in 3.5×10^{-3} mbar of Ar. The base pressure of the chamber is below 5.0×10^{-5} mbar. All samples are exposed to air after each deposition. Subsequently, the samples are loaded in a cold-wall CVD chamber and pumped down to a base pressure of 6.0×10^{-2} mbar. We then set a nominal pressure of 2.5 mbar with 200 sccm NH_3 and heat the samples up to 450 °C at a rate of 3 °C s^{-1} (pretreatment). Upon reaching 450 °C, we replace the NH_3 with 200 sccm C_2H_2 to grow CNTs for 3 min. After the growth, the heater is turned off and C_2H_2 is switched to Ar until the samples are cooled down to room temperature.

2.2 *Sample characterization*

Before the growth of CNTs, we observe the formation of Co nanoparticles on the substrates by scanning electron microscopy (SEM, Hitachi S-5500). The roughness of sample surface is measured by atomic force microscopy (AFM, Veeco Dimension 3100) in tapping mode. The images have been levelled to remove a background tilt. The chemical state of metal films after deposition and after annealing is assessed by XPS. The annealing condition is 450 °C under H_2 at 5×10^{-7} mbar for 10 min. The measurement after annealing is carried out without exposing the samples to air in order to avoid the oxidation. We use the same set up and analyse the spectra with same criteria as previously.[29] We calibrate the binding energies by fixing the C 1*s* peak of contaminants to 284.6 eV. The depth profiles of substrate are analyzed by time-of-flight secondary ion mass spectroscopy (TOF-SIMS, ION-TOF TOF.SIMS 5). We use a Bi liquid metal gun and a Cs ion gun. Bi ions are filtered for Bi_1^+ ions and Cs ions are filtered for Cs^+ ions. The sputtering raster is 300×300 μm^2 using Cs^+ at 500 eV (current 30 nA) and surface spectra are taken from an area of 50×50 μm^2 using Bi_1^+ at 25 keV (target current 1 pA). The guns are operated in high current bunched mode, the

extractor in positive mode, and the analyzer optimized for high mass resolution, acquiring over a range from 0.5 to 740 Da. The depth of the crater is measured using an optical profiling system (Wyko NT1100); it is assumed a constant sputtering rate throughout.

After the growth of CNTs, the samples are observed by SEM and transmission electron microscopy (TEM, JEOL 2200MCO and FEI Tecnai F20). For TEM observation, the samples are transferred to Cu microgrids by scratching the CNT forests on the substrates.

2.3 *Mass density measurement*

We weigh the substrates (1.5 - 4.0 cm^2) before and after CVD process by a microbalance (Satorius ME235S, readability: 0.01 mg). The typical weight gain of the samples by CNT forest is 0.02 - 0.20 mg. The volume of the CNT forests is calculated from the area of the Si substrates and the height of CNT forests. The mass density is calculated from the weight gain of the Si substrates divided by the volume of CNT forests.

2.4 *Electrical and thermal property measurement*

We measure *I-V* characteristics of the CNT forests by conductive AFM (Veeco Dimension 3100 equipped with a Nanoscope V controller). The setup is the same as previously reported.[30] Thermal effusivity is obtained by the picosecond thermoreflectance measurement system.[31] We deposited 100 nm Mo to get better reflectivity from the top surface of the CNT forests. The thermal conductivity is calculated with the thermal effusivity and the specific heat capacity of graphite (0.71 J g^{-1} K^{-1}). The relationship between the thermal effusivity and thermal diffusivity is expressed as

$$b = \sqrt{\lambda c p} \tag{1}$$

where b, λ, c, ρ is thermal effusivity (J m^{-2} $s^{-0.5}$ K^{-1}), thermal diffusivity (J s^{-1} m^{-1} K^{-1}), specific heat capacity (J g^{-1} K^{-1}), and mass density (g cm^{-3}), respectively.

3. Results

Figure 1a shows a side-view SEM image of the substrates after the CVD process. The catalyst condition is shown with a schematic in Figure 1b. The CNT forest with the height of ~300 nm, and the mass density of 1.2 g cm^{-3} grows. As discussed later, 0.50 nm is the optimum thickness for Al layer to grow dense CNT forest with the maximum height. The forest morphology without measurable spacing between tubes (middle inset in Figure 1a) is

completely different from conventional CNT forests. From the top-view image (top inset), the filling factor of the CNT is estimated as ~90%, indicating a very packed morphology for the as-grown forests (without any post processes). The mass density is more than double that of the conventional SWCNT forest after densification by liquid (0.57 g cm^{-3}).[32] The forest and Cu underlayer shows an ohmic behavior with the resistance of 35 ± 26 kΩ (mean ± standard deviation), which indicates the forests have good electrical contact with the conductive support. The lowest value of the resistance is 8.1 kΩ which is better than our previous result by Co-Mo co-catalyst, Figure 1c.[27] As reference, we make the samples without Al and/or Mo, and confirm that the CNT forest grows only when both Al (0.50 nm) and Mo (5.0 nm) are present between Co and Cu (Figure 1d - f). We note that no measurable weight gain is obtained without Co (catalyst) suggesting that other metals (Al, Mo, and Cu) do not catalyze the CNT growth.

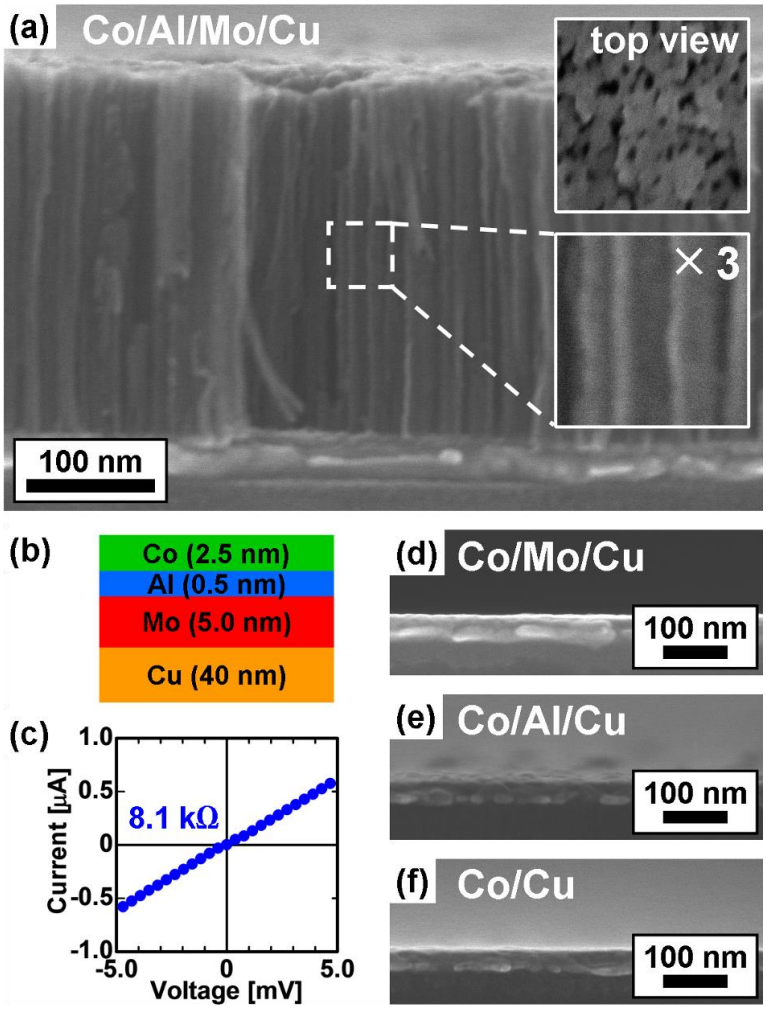

Figure 1. (a) SEM images of the samples with Co/Al/Mo/Cu after CVD process. (b) A schematic of the catalyst condition of (a). (c) A typical *I-V* curve of the CNT forest by

conductive AFM. (d) - (f) SEM images of the samples with different catalyst conditions as references (no CNT growth).

We then characterize the tube structure in detail by TEM and Raman. The diameter distribution of individual tube is wide ranging from 4 to 35 nm with the average diameter of 23 ± 10 nm (mean ± standard deviation). The well-graphitized structures with the lattice spacing of ~0.34 nm are observed (inset in Figure 2a). The Raman spectrum taken from the top of the forest shows G-peak and D-peak which is a typical spectrum for the multi-walled CNTs (Figure 2b). The intensity ratios of G-peak to D-peak (I_G/I_D) is 1.1, which is slightly higher than that of our previous CNT forest by Co-Mo co-catalyst (I_G/I_D = 1.0).[27] Some tubes show inner spacing with ~2 nm (arrow indication in Figure 2a), while the others show no inner spacing (Figure 2c, e-g). The inner spacing of each tube is filled with carbon walls resulting in very solid structure. The average wall number is estimated as 31, assuming that the inner spacing of the tubes with solid structure is 0.34 nm. Most of the catalyst particles are observed at the bottom of the tubes (arrow indication in Figure 2d, g). This is the clear indication that the Co nanoparticles interact strongly with the support resulting in the base growth mechanism. The catalyst particles, with the diameter more than 20 nm, do not have a sphere shape but skewed one by the wall of CNT (arrow indication in Figure 2d). This skewed shape of catalyst particles possibly contributes to grow tubes with extremely narrow inner spacing.

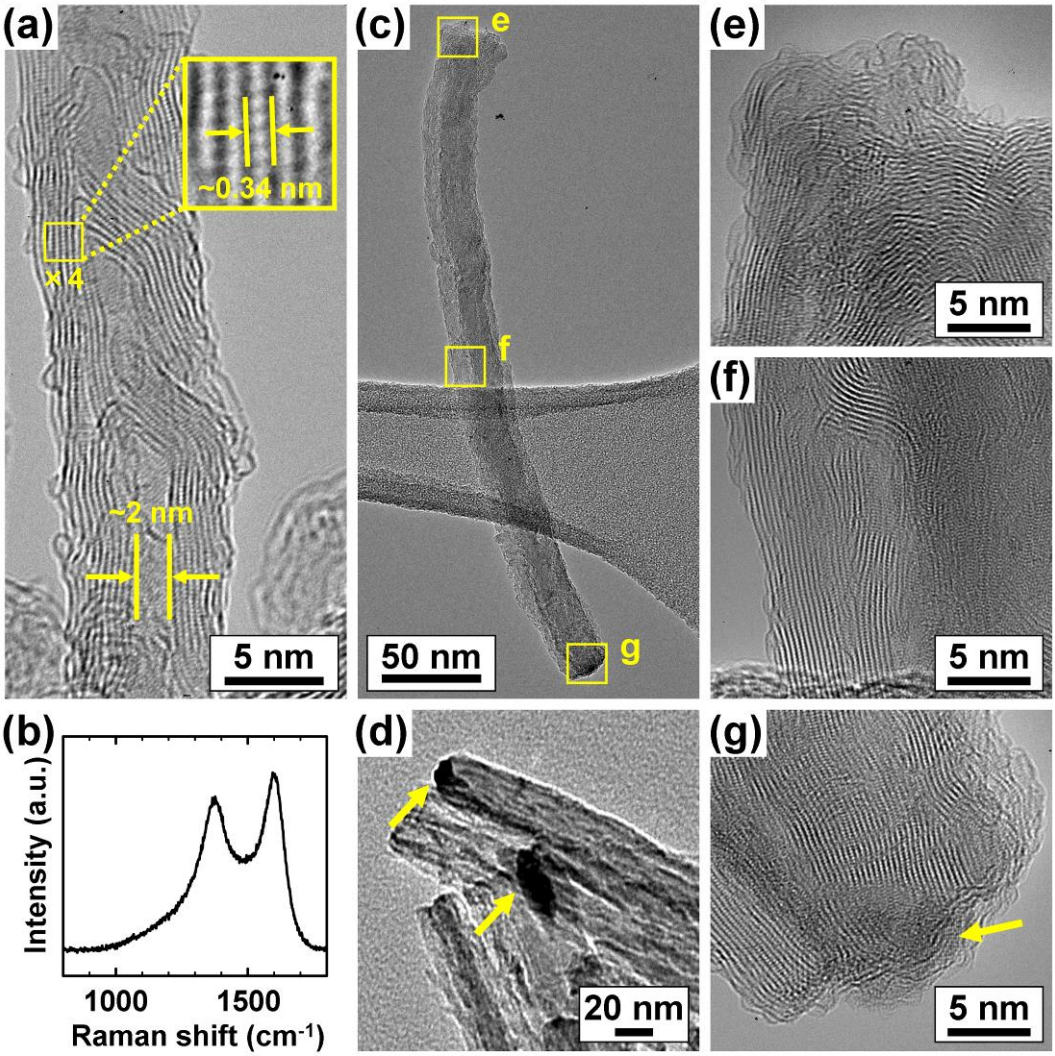

Figure 2. TEM images and Raman spectra of the CNT forest grown by Co/Al/Mo catalyst system. (e), (f), and (g) are the enlarged images of the areas shown with squares in (c), respectively.

It is found that both Al (0.50 nm) and Mo (5.0 nm) are necessary for the dense CNT forest growth (Figure 1). We characterize the formation of Co catalyst nanoparticles under different catalyst conditions. Figure 3 shows the top-view SEM and AFM images of the sample surfaces after the pretreatment at 450 °C under NH_3 (before flowing C_2H_2). With Co/Al/Mo/Cu, where the CNT forest grows, Co form the nanoparticles with the diameter of 9.8 ± 3.0 nm (mean ± standard deviation) and the area density of 1.8×10^{11} cm^{-2}, Figure 3a. The root mean square roughness (R_q) is 1.5 nm indicating the formation of nanoparticles (Figure 3b). On the other hand, Co does not form nanoparticles with Co/Mo/Cu (R_q = 0.44 nm, Figure 3c and 3d), Co/Mo/Cu (R_q = 0.51 nm, Figure 3e and 3f), and Co/Cu (w/o Al and

Mo, R_q = 0.78 nm, Figure 3g and 3h). This is the reason why the CNT forests do not grow on the samples. The results are consistent with the fact that the formation of catalyst nanoparticles is suppressed on conductive supports by their high surface energy.[33-35]

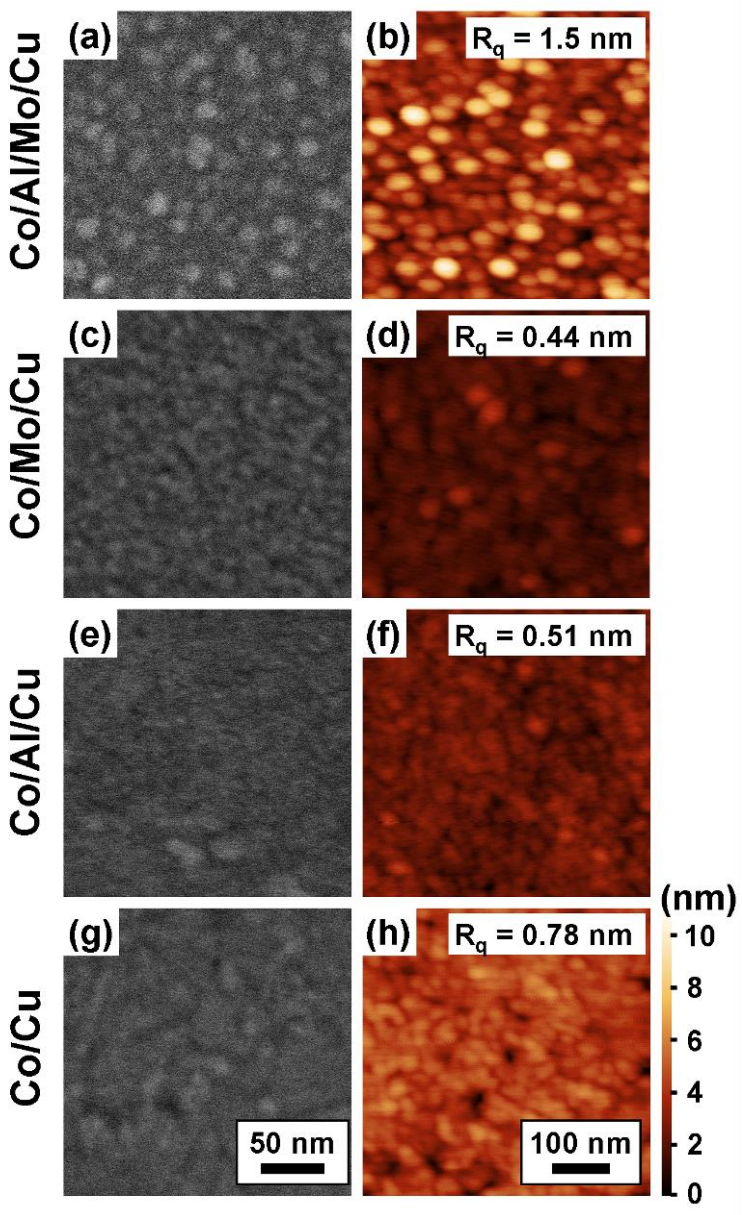

Figure 3 Top-view SEM and AFM images of the catalyst nanoparticles after the pretreatment at 450 °C under NH_3. The scale bars in SEM and AFM images are the same for all the images, respectively.

We then investigate the role of thin Al layer (0.50 nm) measuring the depth profile of the samples by SIMS. We compare the samples with and without Al after pretreatment at

450 °C under NH_3. In the case where the Al layer is present (Figure 4a), we observe clear interfaces between the metal layers. The interfaces of Co/Al/Mo is at ~3 nm, and the Mo/Cu interface at ~9nm. This is largely in agreement with the original heterostructure used. The slight spread of the peaks is due to measurement artefacts such as beam induced mixing and slight tilt of the sample during measurement. When the Al layer is absent, there are no clear interfaces between the Co, Mo, and Cu layers (Figure 4b). This suggests inter-diffusion between the metal layers. We observe both Co and Mo diffusion into the Cu bulk as well as backwards diffusion of Cu towards the surface of the sample. The thin Al layer, even with the thickness of 0.50 nm, clearly prevents the diffusion of Co into Mo layer.

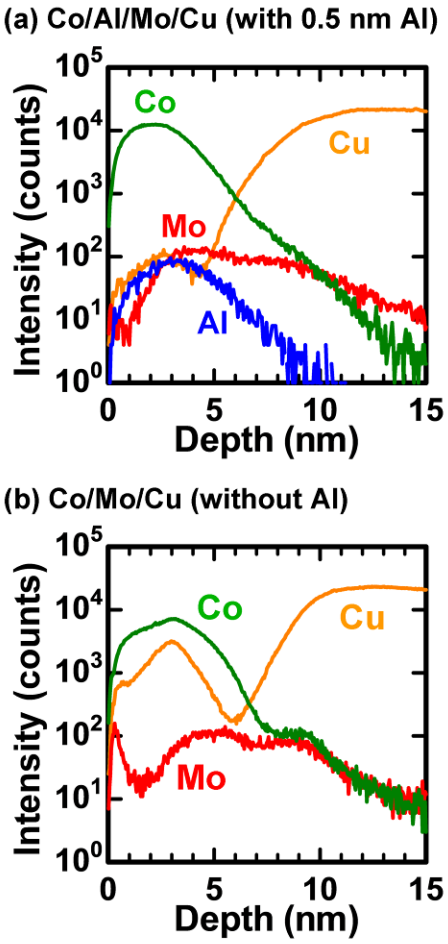

Figure 4. Depth profile of the samples (a) with Al and (b) without Al after annealing at 450 °C under NH_3.

To further assess the effect of Al layer on the catalyst system, we perform XPS characterization on samples with and without Al, and before and after annealing under H_2,

Figure 5. We note that the samples after annealing are not exposed to air before XPS measurement, so we can exclude the possible oxidation in air. XPS shows that after 2.5 nm Co deposition on Mo-coated Cu (i.e. without Al), the Co 2*p* spectrum possesses three main components. They are associated to Co^{2+} (yellow components) at 780.6 eV (Co $2p_{3/2}$) separated by ~15.3 eV from Co $2p_{1/2}$, Co^{3+} (green component) at 783.0 eV separated by ~15.3 eV from Co $2p_{1/2}$, and shake-up losses (black-lined components) at ~786.9 and ~802.5 eV (for Co $2p_{3/2}$ and Co $2p_{1/2}$, respectively) in agreement with literature values.[36] After annealing at 450 °C in H_2, the intensity of the Co^{2+} decreases by a factor of ~2, suggesting the Co film has restructured into nanoparticles. The loss of intensity could also be partly related to inter-diffusion of Co into the Mo-coated Cu layer underneath. The relative intensities of Co^{2+} and Co^{3+} peaks remain nearly constant, suggesting no new compounds have been formed. We note, however, the appearance of a peak centred at 778.0 eV, which corresponds to Co^0. This compares to samples coated with 0.50 nm Al. After deposition, the Co 2*p* lineshape presents the same components as without Al (Co^{2+} and Co^{3+} peaks and the shake-up). After annealing, the total intensity of the Co 2*p* lineshape also decreases by a factor of ~2 (due to nanoparticle formation). However, the intensity of the Co^0 component has increased dramatically with respect to those of the oxides. The Co^0 component at ~778.0 eV dominates the spectrum. This suggests more Co in metallic state is available for nanotube growth after annealing.

These features are also evident on the Mo 3*d* spectra and further help us to understand the role of Al on the formation/stabilization of Co nanoparticles. When we deposit Co without the Al layer, the Mo 3*d* core level shows six main components. They are Mo^0 (red component) at ~228.0 eV, Mo^{2+} (yellow component) at 228.5 eV, Mo^{3+} (green component) at 229.2 eV, Mo^{4+} (purple component) at 230.1 eV, Mo^{5+} (grey component) at 231.6 eV, and Mo^{6+} (pink component) at ~233.0 eV. The oxides have probably been formed during air re-exposure. After annealing the Mo^{2+} (yellow component) at 228.5 eV vanishes, while the Mo^0 and all other oxide components increase their intensities by a factor of ~3. This now compares to Co deposited onto Al. The Mo 3*d* presents a different signature. First, as received samples show no Mo^{2+} component, even though the samples were also exposed to air. Second, after annealing, Mo^0 and all oxide components are present. They are Mo^0 (red component) at ~227.9 eV, Mo^{2+} (yellow component) at 228.5 eV, Mo^{3+} (green component) at 229.2 eV, Mo^{4+} (purple component) at 230.1 eV, Mo^{5+} (grey component) at 231.6 eV, and Mo^{6+} (pink component) at ~233.0 eV. The intensities have increased by a factor of ~2 only. We note that Al is overlapped with Co *3*p peak and too small to observe.

We understand that the presence of Al strongly favours the reduction of Co. After annealing, the peak area ratio of Co^0/Co^{2+} of the sample with Al is ~5 times larger than that without Al. First, Mo^{2+} component is not formed after deposition because Al captures the oxygen and forms Al_2O_x which is much more stable (Al_2O_3: Δ_fG^o = -1582.3 kJ mol^{-1}).[37] Then, during annealing Co restructure into nanoparticles (as shown by AFM) which have larger exposed areas than thin films and therefore easier to reduce. The appearance of Mo^{2+} component is reported when Mo is annealed on Al_2O_3 support.[38]

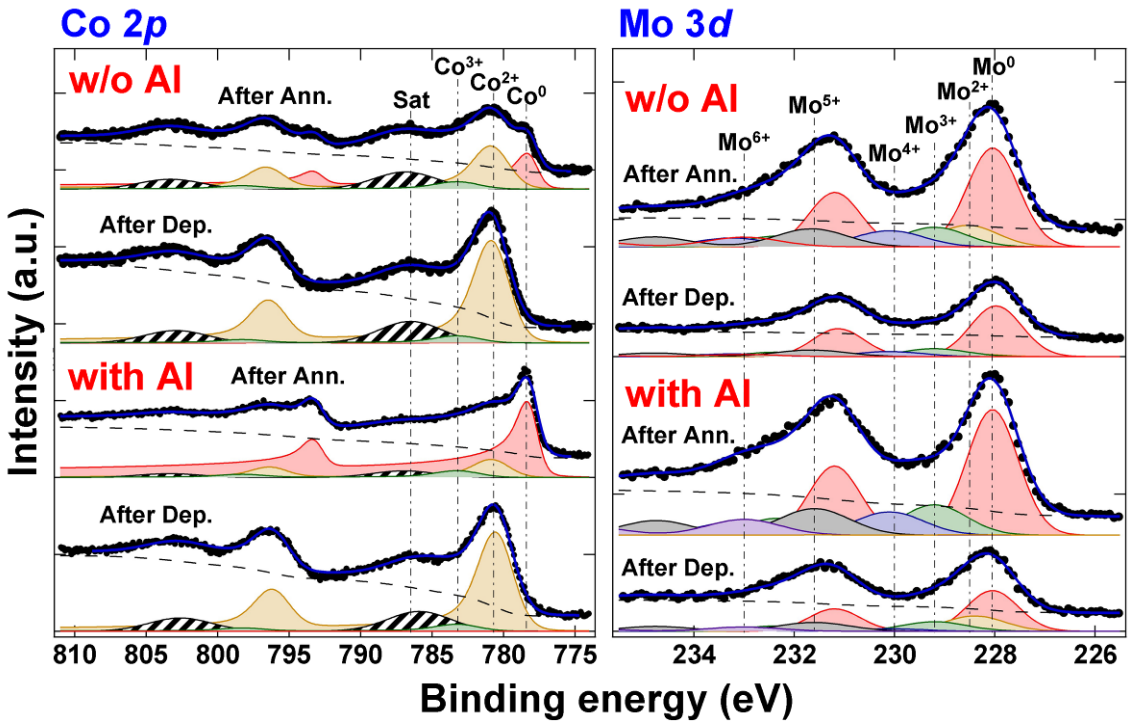

Figure 5. XPS spectra (Co 2*p* and Mo 3*d*) of the samples with and without Al, and before and after annealing at 450 °C for 10 min. The atmosphere during the annealing is H_2 at 5×10^{-7} mbar.

4. Discussion

4.1 *Role of thin Al layer and growth mechanism of tubes with narrow inner spacing*.

It appears that 0.50 nm Al plays an important role to grow the dense CNT forests, although it is much thinner than other metals (Co, Mo, and Cu). As shown with SEM images and schematics in Figure 6, the forest morphology largely depends on Al thickness. The forest height decreases dramatically with 0.25 nm Al (left images in Figure 6a), while the area density of the forest significantly decreases with 1.0 nm Al (right images in Figure 6a).

From these growth results, we conclude that 0.50 nm is the optimum thickness to grow dense CNT forest with the maximum height. We have previously shown that 2.5 nm Co does not grow CNT forests on Mo layer thicker than ~1 nm,[28] and XPS measurement have showed that Co and Mo interact strongly during the CVD process.[27] This strong interaction causes the inter-diffusion of Co and Mo (Figure 4 and 6b), and hinders the formation of Co nanoparticles (from SEM and AFM, Figure 3). This is in agreement with the fact that the forest growth on conductive supports is more challenging than that on insulating supports.[39] The same mechanism will be applied with Co/Cu case herein (without Al and Mo, Figure 1f, 3g, 3h, and 6c). The thin Al layer (0.50 nm), which is most likely oxidized by air exposure, partially prevents the Co-Mo interaction. This helps the formation of Co nanoparticles with high are density (from SEM and AFM, Figure 3), and with more metallic state (from XPS, Figure 5). The forest height decreases with thinner Al (e.g. 0.25 nm) because Co and Mo interact too much (left images in Figure 6a), while when the Al layer is too thick (e.g. 1.0 nm), the forests grow with low area density because the Co-Mo interaction becomes too small (right images in Figure 6a). As shown with the schematic in the right images of Figure 6a, we observe some Co particles lifted off from the substrates and embedded in the tip or the middle of the tubes (data not shown). The lift-off of Co nanoparticles is observed in the case of the forest by Co-Mo on Ti-coated Cu when Mo becomes thin (or without Mo).[27-28] Although the surface energy of Cu (1.56 J m^{-2}) is smaller than that of Mo (2.51 J m^{-2}),[40] the forest does not grow with Co/Al/Cu (without Mo, Figure 1e, 3e, 3f, and 6d). This is most likely because Co does not form a complex carbide or oxide with Cu unlike the case of Co-Mo.[25-26]

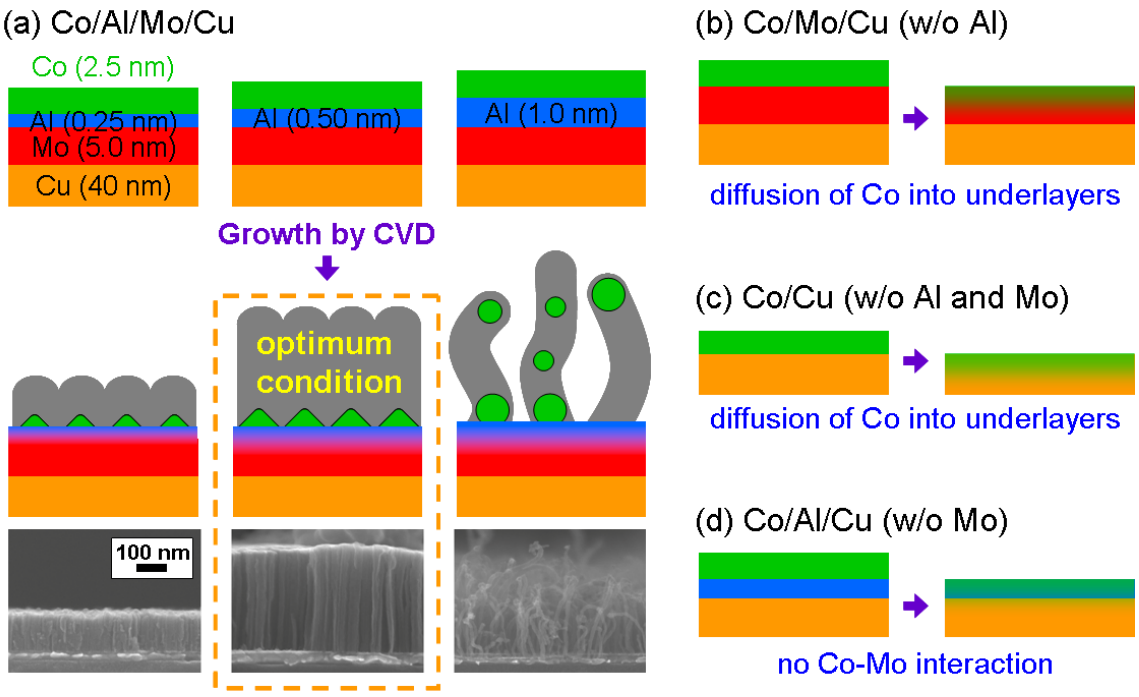

Figure 6. Schematic and SEM images of the growth mechanism of the CNT forest by Co/Al/Mo/Cu catalyst. The scale bar is the same for all the SEM images.

4.2 *Relationship between area density, wall density, and mass density of the CNT forests*.

In the case of conventional tubes, the particle diameter determines the tube diameter. However, most of Co nanoparticles herein do not show sphere shape but skewed one as observed in TEM images (Figure 2). At high temperature (700 - 900 °C), the typical optimum Co thickness for high SWCNT forests is ~0.2 nm with Mo on SiO_2, [41] and ~0.7 nm on aluminium oxide.[19] The Co layer herein (2.5 nm) is more than ~3 times thicker which makes larger particles up to more than 20 nm. These large particles are easier to be skewed by carbon walls to minimize surface energy. This is the reason why some tubes have extremely narrow inner spacing compare to the tubes in conventional CNT forests. In order to integrate as many carbon walls as possible into limited spaces in the CNT forests, either outer spacing (spacing between tubes) or inner spacing (spacing within each tube) have to be reduced. When the outer diameter of the tubes is fixed, the outer spacing can be reduced by increasing area density, while the inner spacing can be reduced by increasing wall number. The area density and the mass density is in a trade-off relationship when the wall density is fixed. For example, when the wall density is the same as 4.1×10^{-12} cm^{-2}, the forest consisting of 31 walls MWCNT with the diameter of 23 nm (mean value for the tubes in this work, Figure 7a) can have mass density of 1.2 g cm^{-3} which is ~6 times higher than that of the forest consisting

of SWCNT with diameter of 2 nm (0.19 g cm^{-3}, Figure 7b). This means that we can integrate more carbon walls into the limited space of CNT forests. The MWCNT forest with relatively large diameter can be applied for heat dissipation devices. On the other hand, SWCNT (or few layer CNT) forest with small diameter can be used for electrical conduction channels since each tubes have more uniform quantum resistance. By optimizing the catalyst thickness and growth condition, we manages to grow the forest filling the unused spacing in each tube as shown the graph in Figure 7c. The values for conventional tubes are calculated based on the paper by Chiodarelli et al.[42] This narrow inner spacing possibly comes from the skewed catalyst particles as mentioned in the previous section (4.1).

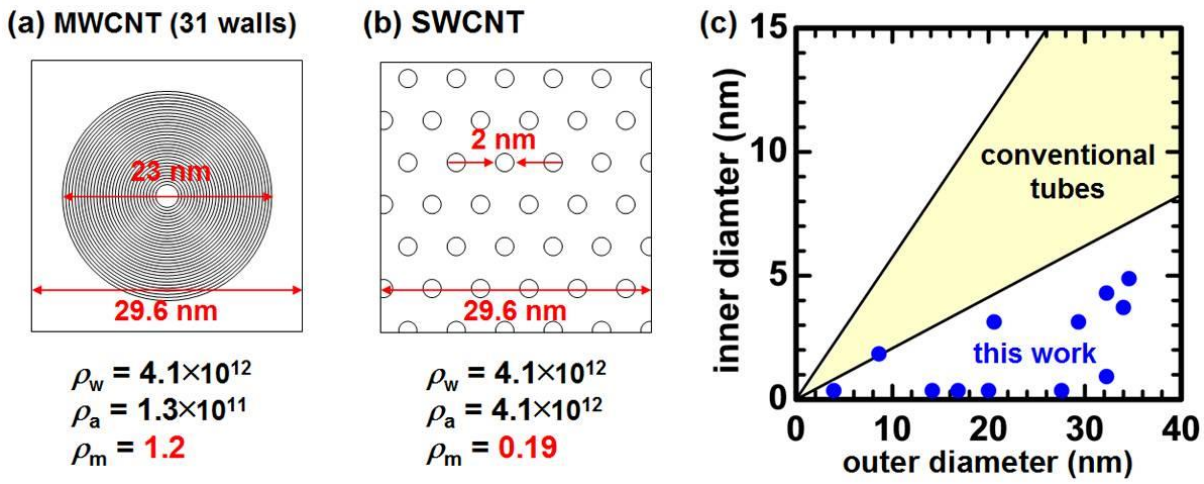

Figure 7. Schematics of and summarized properties of CNT forests with (a) 31 walls MWCNT (diameter: 23 nm), and (b) SWCNT (diameter: 2 nm). ρ_w, ρ_a, ρ_m are wall density (cm^{-2}), area density (cm^{-2}), and mass density (g cm^{-3}), respectively. (c) Relationship between outer tube diameter and inner diameter, comparing the tubes in this work with conventional tubes. The data for conventional tubes is based on the paper by Chiodarelli et al.[42]

4.3 *Thermal properties of the CNT forests.*

Finally, the thermal property of the CNT forest is measured by the picosecond thermoreflectance measurement system.[31] The forest shows the thermal effusivity of 1840 J m^{-2} $s^{-0.5}$ K and thermal conductivity of 4.0 J s^{-1} m^{-1} K^{-1}, which is ~2 and ~4 times higher than that reported with as-grown dense vertical graphene layers (975 J m^{-2} $s^{-0.5}$ K^{-1}, and 1.0 J m^{-1} s^{-1} K^{-1}), respectively.[31] The forest herein does not have horizontal graphene layers on top as they reported, so it shows the high thermal effusivity even with as-grown samples. These

forests are potentially useful for heat dissipation devices. We summarize the properties of the CNT forests comparing with the forests grown with Co-Mo catalyst on Ti-coated Cu.[27]

	Co/Al/Mo/Cu	Co/Mo/Ti/Cu
Height	300	380 *
Mass density (g cm^{-3})	1.2	1.6 *
Resistance (kΩ)	35 ± 26	95 ± 46 *
Thermal effusivity ($J\ m^{-2}\ s^{-0.5}\ K^{-1}$)	1840	2100
Thermal conductivity ($J\ s^{-1}\ m^{-1}\ K^{-1}$)	4.0	3.9

Table 1. Properties of CNT forests grown with Co/Al/Mo/Cu catalyst system (this work), comparing with the forest grown with Co/Mo/Ti/Cu catalyst.[27]
(* data from our previous paper[27])

5. Conclusion

We grow carbon nanotube forests at 450 °C on conductive Cu support with tubes exhibiting extremely narrow inner spacing using Co/Al/Mo multilayer catalyst system. The 0.50 nm Al layer acts as a barrier layer which partially prevents the interaction between Co and Mo. This thin Al layer helps Co nanoparticles formation with high area density. The forests average ~300 nm in height and a mass density of 1.2 g cm^{-3}. An ohmic behavior is confirmed between the forest and Cu support with the resistance of 35 ± 26 kΩ (mean ± standard deviation). The forest shows a high thermal effusivity of 1840 $J\ m^{-2}\ s^{-0.5}\ K^{-1}$, and the thermal conductivity is 4.0 $J\ s^{-1}\ m^{-1}\ K^{-1}$, suggesting that these forests are potentially useful for heat dissipation devices.

Acknowledgement

This work has been funded by the European projects Technotubes and Grafol. H.S. acknowledges a research fellowship from the Japanese Society for the Promotion of Science (JSPS).

References

(1) Yao, Z.; Kane, C. L.; Dekker, C., High-Field Electrical Transport in Single-Wall Carbon Nanotubes. *Phys. Rev. Lett.* **2000,** *84*, 2941-2944.

(2) Berber, S.; Kwon, Y. K.; Tomanek, D., Unusually High Thermal Conductivity of Carbon Nanotubes. *Phys. Rev. Lett.* **2000,** *84*, 4613-4616.

(3) Kim, P.; Shi, L.; Majumdar, A.; McEuen, P. L., Thermal Transport Measurements of Individual Multiwalled Nanotubes. *Phys. Rev. Lett.* **2001,** *87*, 215502.

(4) Park, J. Y.; Rosenblatt, S.; Yaish, Y.; Sazonova, V.; Ustunel, H.; Braig, S.; Arias, T. A.; Brouwer, P. W.; McEuen, P. L., Electron-Phonon Scattering in Metallic Single-Walled Carbon Nanotubes. *Nano Lett.* **2004,** *4*, 517-520.

(5) Kreupl, F.; Graham, A. P.; Duesberg, G. S.; Steinhogl, W.; Liebau, M.; Unger, E.; Honlein, W., Carbon Nanotubes in Interconnect Applications. *Microelectron. Eng.* **2002,** *64*, 399-408.

(6) Naeemi, A.; Meindl, J. D., Compact Physical Models for Multiwall Carbon-Nanotube Interconnects. *IEEE Electron Device Lett.* **2006,** *27*, 338-340.

(7) Ngo, Q.; Cruden, B. A.; Cassell, A. M.; Sims, G.; Meyyappan, M.; Li, J.; Yang, C. Y., Thermal Interface Properties of Cu-Filled Vertically Aligned Carbon Nanofiber Arrays. *Nano Lett.* **2004,** *4*, 2403-2407.

(8) Cantoro, M.; Hofmann, S.; Pisana, S.; Scardaci, V.; Parvez, A.; Ducati, C.; Ferrari, A. C.; Blackburn, A. M.; Wang, K. Y.; Robertson, J., Catalytic Chemical Vapor Deposition of Single-Wall Carbon Nanotubes at Low Temperatures. *Nano Lett.* **2006,** *6*, 1107-1112.

(9) Shang, N. G.; Tan, Y. Y.; Stolojan, V.; Papakonstantinou, P.; Silva, S. R. P., High-Rate Low-Temperature Growth of Vertically Aligned Carbon Nanotubes. *Nanotechnology* **2010,** *21*, 505604.

(10) Nihei, M.; Kawabata, A.; Awano, Y., Direct Diameter-Controlled Growth of Multiwall Carbon Nanotubes on Nickel-Silicide Layer. *Jpn. J. Appl. Phys. Part 2 - Lett.* **2003,** *42*, L721-L723.

(11) Yokoyama, D.; Iwasaki, T.; Ishimaru, K.; Sato, S.; Hyakushima, T.; Nihei, M.; Awano, Y.; Kawarada, H., Electrical Properties of Carbon Nanotubes Grown at a Low Temperature for Use as Interconnects. *Jpn. J. Appl. Phys.* **2008,** *47*, 1985-1990.

(12) Na, N.; Kim, D. Y.; So, Y. G.; Ikuhara, Y.; Noda, S., Simple and Engineered Process Yielding Carbon Nanotube Arrays with 1.2 X 10(13) Cm(-2) Wall Density on Conductive Underlayer at 400 Degrees C. *Carbon* **2015,** *81*, 773-781.

(13) Huang, J. Y.; Chen, S.; Jo, S. H.; Wang, Z.; Han, D. X.; Chen, G.; Dresselhaus, M. S.; Ren, Z. F., Atomic-Scale Imaging of Wall-by-Wall Breakdown and Concurrent Transport Measurements in Multiwall Carbon Nanotubes. *Phys. Rev. Lett.* **2005,** *94*, 236802.

(14) Hata, K.; Futaba, D. N.; Mizuno, K.; Namai, T.; Yumura, M.; Iijima, S., Water-Assisted Highly Efficient Synthesis of Impurity-Free Single-Waited Carbon Nanotubes. *Science* **2004,** *306*, 1362-1364.

(15) Zhong, G. F.; Iwasaki, T.; Honda, K.; Furukawa, Y.; Ohdomari, I.; Kawarada, H., Low Temperature Synthesis of Extremely Dense, and Vertically Aligned Single-Walled Carbon Nanotubes. *Japanese Journal of Applied Physics Part 1-Regular Papers Short Notes & Review Papers* **2005,** *44*, 1558-1561.

(16) Noda, S.; Hasegawa, K.; Sugime, H.; Kakehi, K.; Zhang, Z. Y.; Maruyama, S.; Yamaguchi, Y., Millimeter-Thick Single-Walled Carbon Nanotube Forests: Hidden Role of Catalyst Support. *Jpn. J. Appl. Phys. Part 2 - Lett. Express Lett.* **2007,** *46*, L399-L401.

(17) Chakrabarti, S.; Kume, H.; Pan, L. J.; Nagasaka, T.; Nakayama, Y., Number of Walls Controlled Synthesis of Millimeter-Long Vertically Aligned Brushlike Carbon Nanotubes. *J. Phys. Chem. C* **2007,** *111*, 1929-1934.

(18) Ohno, H.; Takagi, D.; Yamada, K.; Chiashi, S.; Tokura, A.; Homma, Y., Growth of Vertically Aligned Single-Walled Carbon Nanotubes on Alumina and Sapphire Substrates. *Japanese Journal of Applied Physics Part 1-Regular Papers Short Notes & Review Papers* **2008,** *47*, 1956-1960.

(19) Sugime, H.; Noda, S., Millimeter-Tall Single-Walled Carbon Nanotube Forests Grown from Ethanol. *Carbon* **2010,** *48*, 2203-2211.

(20) Zhong, G. F.; Warner, J. H.; Fouquet, M.; Robertson, A. W.; Chen, B. A.; Robertson, J., Growth of Ultrahigh Density Single-Walled Carbon Nanotube Forests by Improved Catalyst Design. *ACS Nano* **2012,** *6*, 2893-2903.

(21) Murakami, Y.; Chiashi, S.; Miyauchi, Y.; Hu, M. H.; Ogura, M.; Okubo, T.; Maruyama, S., Growth of Vertically Aligned Single-Walled Carbon Nanotube Films on Quartz Substrates and Their Optical Anisotropy. *Chem. Phys. Lett.* **2004,** *385*, 298-303.

(22) Christen, H. M.; Puretzky, A. A.; Cui, H.; Belay, K.; Fleming, P. H.; Geohegan, D. B.; Lowndes, D. H., Rapid Growth of Long, Vertically Aligned Carbon Nanotubes through Efficient Catalyst Optimization Using Metal Film Gradients. *Nano Lett.* **2004,** *4*, 1939-1942.

(23) Noda, S.; Sugime, H.; Osawa, T.; Tsuji, Y.; Chiashi, S.; Murakami, Y.; Maruyama, S., A Simple Combinatorial Method to Discover Co-Mo Binary Catalysts That Grow Vertically Aligned Single-Walled Carbon Nanotubes. *Carbon* **2006,** *44*, 1414-1419.

(24) Zhang, L.; Tan, Y. Q.; Resasco, D. E., Controlling the Growth of Vertically Oriented Single-Walled Carbon Nanotubes by Varying the Density of Co-Mo Catalyst Particles. *Chem. Phys. Lett.* **2006,** *422*, 198-203.

(25) Herrera, J. E.; Balzano, L.; Borgna, A.; Alvarez, W. E.; Resasco, D. E., Relationship between the Structure/Composition of Co-Mo Catalysts and Their Ability to Produce Single-Walled Carbon Nanotubes by Co Disproportionation. *Journal of Catalysis* **2001,** *204*, 129-145.

(26) Hu, M. H.; Murakami, Y.; Ogura, M.; Maruyama, S.; Okubo, T., Morphology and Chemical State of Co-Mo Catalysts for Growth of Single-Walled Carbon Nanotubes Vertically Aligned on Quartz Substrates. *Journal of Catalysis* **2004,** *225*, 230-239.

(27) Sugime, H.; Esconjauregui, S.; Yang, J. W.; D'Arsie, L.; Oliver, R. A.; Bhardwaj, S.; Cepek, C.; Robertson, J., Low Temperature Growth of Ultra-High Mass Density Carbon Nanotube Forests on Conductive Supports. *Appl. Phys. Lett.* **2013,** *103*, 073116.

(28) Sugime, H.; Esconjauregui, S.; D'Arsie, L.; Yang, J. W.; Makaryan, T.; Robertson, J., Growth Kinetics and Growth Mechanism of Ultrahigh Mass Density Carbon Nanotube Forests on Conductive Ti/Cu Supports. *ACS Appl. Mater. Interfaces* **2014,** *6*, 15440-15447.

(29) Esconjauregui, S.; Cepek, C.; Fouquet, M.; Bayer, B. C.; Gamalski, A. D.; Chen, B. A.; Xie, R. S.; Bhardwaj, S.; Ducati, C.; Hofmann, S.; Robertson, J., Plasma Stabilisation of Metallic Nanoparticles on Silicon for the Growth of Carbon Nanotubes. *J. Appl. Phys.* **2012,** *112*, 034303.

(30) Bayer, B. C.; Zhang, C.; Blume, R.; Yan, F.; Fouquet, M.; Wirth, C. T.; Weatherup, R. S.; Lin, L.; Baehtz, C.; Oliver, R. A.; Knop-Gericke, A.; Schlogl, R.; Hofmann, S.; Robertson, J., In-Situ Study of Growth of Carbon Nanotube Forests on Conductive Cosi(2) Support. *J. Appl. Phys.* **2011,** *109*, 114314.

(31) Kawabata, A.; Murakami, T.; Nihei, M.; Yokoyama, N., Growth of Dense, Vertical and Horizontal Graphene and Its Thermal Properties. *Jpn. J. Appl. Phys.* **2013,** *52*, CB406-CB406.

(32) Futaba, D. N.; Hata, K.; Yamada, T.; Hiraoka, T.; Hayamizu, Y.; Kakudate, Y.; Tanaike, O.; Hatori, H.; Yumura, M.; Iijima, S., Shape-Engineerable and Highly Densely Packed Single-Walled Carbon Nanotubes and Their Application as Super-Capacitor Electrodes. *Nat. Mater.* **2006,** *5*, 987-994.

(33) Wang, Y. Y.; Luo, Z. Q.; Li, B.; Ho, P. S.; Yao, Z.; Shi, L.; Bryan, E. N.; Nemanich, R. J., Comparison Study of Catalyst Nanoparticle Formation and Carbon Nanotube Growth: Support Effect. *J. Appl. Phys.* **2007,** *101*, 124310.

(34) Dijon, J.; Fournier, A.; Szkutnik, P. D.; Okuno, H.; Jayet, C.; Fayolle, M., Carbon Nanotubes for Interconnects in Future Integrated Circuits: The Challenge of the Density. *Diam. Relat. Mat.* **2010,** *19*, 382-388.

(35) Esconjauregui, S.; Bayer, B. C.; Fouquet, M.; Wirth, C. T.; Yan, F.; Xie, R.; Ducati, C.; Baehtz, C.; Castellarin-Cudia, C.; Bhardwaj, S.; Cepek, C.; Hofmann, S.; Robertson, J., Use of Plasma Treatment to Grow Carbon Nanotube Forests on Tin Substrate. *J. Appl. Phys.* **2011,** *109*, 114312.

(36) Briggs, D.; Grant, J., *Surface Analysis by Auger and Xray Photoelectron Spectroscopy (IM Publications, Chickester, UK, 2003).*

(37) Haynes, W. M., *CRC Handbook of Chemisty and Physics 95th ed.* **2014**.

(38) Zaki, M. I.; Vielhaber, B.; Knozinger, H., Low-Temperature Co Adsorption and State of Molybdena Supported on Alumina, Titania, Ceria, and Zirconia - an Infrared Spectroscopic Investigation. *Journal of Physical Chemistry* **1986,** *90*, 3176-3183.

(39) Robertson, J.; Zhong, G. F.; Esconjauregui, C. S.; Bayer, B. C.; Zhang, C.; Fouquet, M.; Hofmann, S., Applications of Carbon Nanotubes Grown by Chemical Vapor Deposition. *Jpn. J. Appl. Phys.* **2012,** *51*, 01AH01.

(40) Tyson, W. R.; Miller, W. A., Surface Free-Energies of Solid Metals - Estimation from Liquid Surface-Tension Measurements. *Surf. Sci.* **1977,** *62*, 267-276.

(41) Sugime, H.; Noda, S.; Maruyama, S.; Yamaguchi, Y., Multiple "Optimum" Conditions for Co-Mo Catalyzed Growth of Vertically Aligned Single-Walled Carbon Nanotube Forests. *Carbon* **2009,** *47*, 234-241.

(42) Chiodarelli, N.; Richard, O.; Bender, H.; Heyns, M.; De Gendt, S.; Groeseneken, G.; Vereecken, P. M., Correlation between Number of Walls and Diameter in Multiwall Carbon Nanotubes Grown by Chemical Vapor Deposition. *Carbon* **2012,** *50*, 1748-1752.